Polysaccharide of *Atractylodes macrocephala* Koidz alleviate lipopolysaccharide-induced liver injury in goslings via the p53 and FOXO pathways

Bingqi Zhang,[*,†] Longsheng Hong,[†] Jingfei Ke,[*] Yueyun Zhong,[*,†] Nan Cao,[*,†] Wanyan Li,[*,†] Danning Xu,[*,†] Yunbo Tian,[*,†] Yunmao Huang,[*,†] Wenbin Chen,[*,†] and Bingxin Li[*,†,1]

[*]*College of Animal Science & Technology, Zhongkai University of Agriculture and Engineering, Guangzhou 510225, China; and [†]Guangdong Province Key Laboratory of Waterfowl Healthy Breeding, Guangzhou 510225, China*

ABSTRACT Lipopolysaccharide (**LPS**) can affect the immune system of geese by inducing liver injury. The polysaccharide of *Atractylodes macrocephala* Koidz (**PAMK**) have obvious immune-enhancing effects. Accordingly, this experiment investigated the effect of PAMK on LPS-induced liver injury in goslings. Two hundred 1-day-old goslings were randomly divided into the control group, LPS group, PAMK group, and PAMK+ LPS group, and the PAMK and PAMK+ LPS groups were fed the basal diet with 400 mg/kg PAMK, while the control and LPS groups were fed the basal diet. On D 21, 23, and 25 of the formal trial, the goslings in the LPS and PAMK +LPS groups were injected intraperitoneally with 2 mg/kg LPS, and goslings in the control and PAMK groups were injected intraperitoneally with the same amount of saline. Livers were collected on D 25. HE-stained sections showed that PAMK could effectively alleviate the LPS-induced indistinct hepatic cord structure, loss of cytoplasmic contents of hepatocytes, and dilatation of hepatic sinusoids. The biochemical parameters of liver tissues showed that PAMK could alleviate the LPS-induced upregulation of alanine aminotransferase and aspartate aminotransferase. To further investigate the mechanism of the mitigating effect of PAMK on LPS-induced injury, livers from the LPS and PAMK+LPS groups were selected for transcriptome sequencing. The sequencing results showed that there were 406 differentially expressed genes (**DEGs**) in the livers of LPS and PAMK+LPS goslings, of which 242 upregulated and 164 downregulated. The Kyoto Encyclopedia of Genes and Genome (**KEGG**) analysis showed that DEGs were significantly enriched in immune signal transduction, cell cycle, and cell metabolism. Besides, protein–protein interaction analysis showed that 129 DEGs were associated with each other, including 7 DEGs enriched in the p53 and FOXO signaling pathway. In conclusion, PAMK may alleviate LPS-induced liver injury in gosling through the p53 and FOXO signaling pathway. These results provide a basis for further development of PAMK as an immunomodulator.

Key words: lipopolysaccharide, polysaccharide of *Atractylodes macrocephala* Koidz, gene expression, liver, gosling

INTRODUCTION

Lipopolysaccharide (**LPS**) is an important pathogenic factor of gram-negative bacteria and is a pathogen-associated molecular pattern (Bowen et al., 2009). LPS rarely shows symptoms at the beginning of its entry into the body, but as it spends more time in the body, many adverse effects gradually appear (Beutler, 2004; Bilodeau-Bourgeois et al., 2008). During waterfowl farming, the aquatic environment tends to harbor harmful bacteria, resulting in elevated concentrations of LPS in the organism. LPS stimulates the innate immune response, inducing cells to produce and release a series of inflammatory mediators, causing toxicity to spread in the body and accelerating the inflammatory process (Xi et al., 2019). For example, LPS can induce an inflammatory response in ducks and cause damage to the intestinal tract (Yang et al., 2021; Liu et al., 2022; Qin et al., 2022).

The liver is an organ in the body with a predominantly metabolic function and is also an important intrinsic immune organ. Due to the existence of the "gut liver axis," the liver continuously metabolizes LPS from the gut to maintain the body's immune level. Research

has found that excess LPS can cause the liver to undergo pathological changes, which in turn induces liver inflammation (Ding et al., 2018). In patients with acute liver failure, the liver's ability to clear LPS is reduced, leading to increased release of inflammatory cytokines and increased liver function damage (Chastre et al., 2014). LPS can promote the activation of hepatic stellate cells and their transformation into myofibroblasts, which are involved in the formation of liver fibrosis (Quiroz et al., 2001). It has also been suggested that inflammatory mediators released by LPS can increase the chance of neurological complications from liver disease (Lindros et al., 2005).

In previous studies, polysaccharide of *Atractylodes macrocephala* Koidz (**PAMK**) have been shown to have significant anti-inflammatory and antioxidant effects (Xu et al., 2015; Li et al., 2019). PAMK can slow LPS-induced splenic ferroptosis (Li et al., 2022) and maintain small intestinal morphology in goslings, improve intestinal flora disorders, and alleviate LPS-induced enteritis in goslings (Li et al., 2021). Meanwhile, PAMK also has a protective effect on the liver by regulating antioxidant enzyme activity and hepatic lipid metabolism to improve liver injury induced by high-energy and low protein diets (Miao et al., 2021) and mediates signaling pathways to reduce liver inflammatory damage and oxidative stress (Guo et al., 2021). However, the effect of PAMK on LPS-induced liver damage in goslings has not been reported. Therefore, in this study, we tried to investigate the effect of PAMK on LPS-induced liver injury in goslings by establishing a model of LPS-induced liver injury in goslings and to understand the mechanisms involved in the protective effect of PAMK against LPS-induced liver injury in goslings by transcriptome sequencing data.

MATERIAL AND METHODS

Ethics Statement

In this study, all Magang goslings (Anser cygnoides) were treated humanely, and the experiment was approved by Zhongkai University of Agriculture and Engineering.

Experimental Animals and Sample Preparation

PAMK was purchased from Tianyuan (purity 95%, Yanglingciyuan Biotechnology Company, Xi'an, China). The goslings were purchased from Jinye Bird Breeding (Guangdong) Co., Ltd. A total of 200 goslings were reared, half of which were males and half of which were females. They participated in the experiment at 0 d of age, were prefed for 3 d, and then entered the formal trial, which lasted 25 d. These goslings were randomly divided into 4 groups of 50 birds each. These four groups of goslings had free access to food (including vegetables) and water. The control and LPS groups were fed normal diets, and the PAMK and PAMK + LPS groups were fed normal diets supplemented with PAMK 400 mg·kg^{-1}. In addition, at D 21, 23, and 25 of the formal trial, intraperitoneal injection of saline 0.5 mL was performed in the control and PAMK groups, and intraperitoneal injection of LPS (L2880, Sigma, MO) 2 mg/(kg body weight) was started in the LPS and PAMK + LPS groups once a day. Livers were collected on D 25 of the formal trial. Painless execution of all goslings after anesthesia. All samples were immediately placed in liquid nitrogen and stored at −80°C.

Histomorphological Observation of the Liver

Fresh liver tissue was washed with normal saline three times, and the water on the surface of the tissue was wiped away. It was fixed in a 10% neutral buffered formalin solution for 48 h, embedded in paraffin, and cut into 5 to 6 μm thick slices. A routine histological examination was performed, and paraffin sections were stained with HE. HE-stained sections were analyzed under a Nikon fluorescence microscope (Nikon, Tokyo, Japan).

Detection of Biochemical Indicators in the Liver

In the test, 0.1 g of liver tissue was cut, and 0.9 mL of normal saline was added. After crushing with a crusher, the samples were centrifuged at 2000 × g for 5 min, and the supernatant was collected for use. The levels of alanine aminotransferase (**ALT**) and aspartate aminotransferase (**AST**) in the tissue supernatant were measured using kits (C009-2-1, C010-2-1, Nanjing Jiancheng Bioengineering Institute, Nanjing, China).

RNA Extraction and Library Construction

To further investigate the mechanism of action of PAMK on LPS-induced liver injury. Three samples of liver tissue from each of the LPS and PAMK + LPS groups of goslings were taken for high-throughput sequencing. RNA from total samples was isolated and purified using TRIzol (15596018, Invitrogen, CA) according to the instructions provided by the manufacturer. The purity of the RNA samples was determined by measuring OD260/280 values in the ranges of 1.8 to 2.0 and RIN > 7.0. RNA purity was verified by agarose gel electrophoresis, and RNA integrity was detected using a Bioanalyzer 2100 system (5067-1511, Agilent CA). The captured mRNA was fragmented using a magnesium ion interruption kit (cat.E6150S, NEBNext Magnesium RNA Fragmentation Module, USA) at 94°C for 5 to 7 min under high temperature conditions. Fragmented RNA was synthesized into cDNA by reverse transcriptase (cat. 1896649, Invitrogen SuperScript II Reverse Transcriptase, CA). The duplexes of DNA and RNA were transformed into DNA duplexes and mixed with dUTP Solution (item #R0133, Thermo Fisher, CA), and the ends of the double-stranded DNA were

aligned to flat ends. The fragment size was screened and purified using oligo (dT) magnetic beads (Dynabeads Oligo (dT)). The second strand was digested with UDG enzymes (cat.m0280, NEB, MA) and subjected to PCR to make a library with a fragment size of 300 bp $\pm$ 50 bp. All cDNAs were double-end sequenced using an Illumina Novaseq 6000 (LC Bio Technology CO., Ltd. Hangzhou, China) in PE150 sequencing mode according to standard practices.

Identification of Differentially Expressed Genes (DEGs)

To obtain high-quality clean reads, Cutadapt (https://eutadapt.readthedocs.io/en/stable/, version: cutadapt-1.9) filters the reads further. Quality control of the downstream raw data, including Q20, Q30, and GC content of the clean data, was performed using FASTQ software (https://github.com/OpenGene/fastp). Sequencing data were aligned to the genome (Homo sapiens, GRCh38) using HISAT2 (https://ccb.jhu.edu/software/hisat2). The assembly of genes or transcripts was performed using StringTie software (https://ccb.jhu.edu/software/hisat2). Quantification by FPKM (FPKM = total_exon_fragments/[mapped_reads (millions) × exon_length(kB)]) was performed using the R package edgeR (https://bioconductor.org/packages/release/bioc/html/edgeR.html) and was analyzed for DEGs between samples. DEGs were assessed by determining the two criteria of more than twofold change in expression and P value < 0.05.

Gene Ontology (GO) and Kyoto Encyclopedia of Genes and Genome (KEGG) Enrichment Analysis

GO is an internationally standardized gene function classification system that comprehensively characterizes the genes and their products in an organism. KEGG is a database for the systematic analysis of gene function and can link gene information to biofunctional information. In this experiment, all DEGs were enriched for the GO function using the Goseq R package. KEGG functional enrichment analysis was performed using the KOBAS online tool (http://kobas.cbi.pku.edu.cn/genelist/). The 50 GO terms enriched, and the 15 enrichment pathway analysis results of KEGG were visualized.

Protein–protein Interaction (PPI)) Network

The STRING 10 database (http://string-db.org/), a search tool for retrieving interacting genes, was used to determine the relationships at the protein level of the DEGs involved in the PAMK mitigation of the LPS-induced liver injury pathway in goslings. Meanwhile, this experiment screened the enriched genes in the pathway related to PAMK alleviation of LPS-induced liver injury in goslings within the database. The results were visualized using Cytoscape v3.2.1.

Validation of RNA Sequencing (RNA-Seq) Results Using qRT–PCR

Seven DEGs in a significantly enriched pathway associated with PAMK alleviation of LPS-induced liver injury in goslings were selected by qRT–PCR to validate the results of performing high-throughput RNA-seq analysis as described previously. Five liver samples were selected from each group of the same batch, and total RNA was extracted using TRIzol reagent (GK20008, Glpbio, CA) and reverse transcribed according to the instructions of the TaKaRa Reverse Transcription Kit (RR036A, Takara, Beijing, China). Quantitative reverse transcription polymerase chain reaction analysis was performed on a real-time fluorescence quantitative PCR instrument (7500) (Life Technologies, Singapore) using 2 × RealStar Fast SYBR qPCR Mix (A304-01, GenStar, Beijing, China) with the following reaction system: SYBR Green Master Mix 10 μL, RNase Free dH$_2$O 7 μL, F Primer 1 μL, P Primer 1 μL, and cDNA 1 μL. The reaction procedure of quantitative reverse transcription polymerase chain reaction was as follows: predenaturation at 95°C for 5 min; denaturation at 95°C for 30 s, annealing at 60°C for 30 s, extension at 72°C for 30 s, and extension at 72°C for 10 min. The relative expression levels of mRNA of the target genes were calculated using the $2^{-\Delta\Delta CT}$ method with $ACTB$ as the internal reference gene.

Statistical Data Analysis

Data are expressed as the mean ± standard error (**SEM**). One-way ANOVA was performed using SPSS 26.0 statistical software, multiple comparisons were performed using the Tukey method, and significance tests were performed for biochemical indicators. Two-tailed Student's t test was performed with SPSS 26.0 statistical software to test the significance of Log2 RNA-Seq versus Log2 qRT–PCR for DEGs in the LPS and PAMK + LPS groups. GraphPad Prism 5.0 was used to visualize the data. P < 0.05 was considered significant.

RESULTS

PAMK Alleviates LPS-induced Liver Injury in Goslings

HE-stained sections of gosling livers from all treatment groups were compared with the control group (Figure 1). Compared with the control group, the LPS group showed poorly defined hepatic cord structure, loss of hepatocyte cytoplasmic contents, and dilated hepatic sinusoids. In contrast, the hepatic cords in the PAMK and PAMK+LPS groups were neatly arranged, with normal hepatocyte structure and morphology.
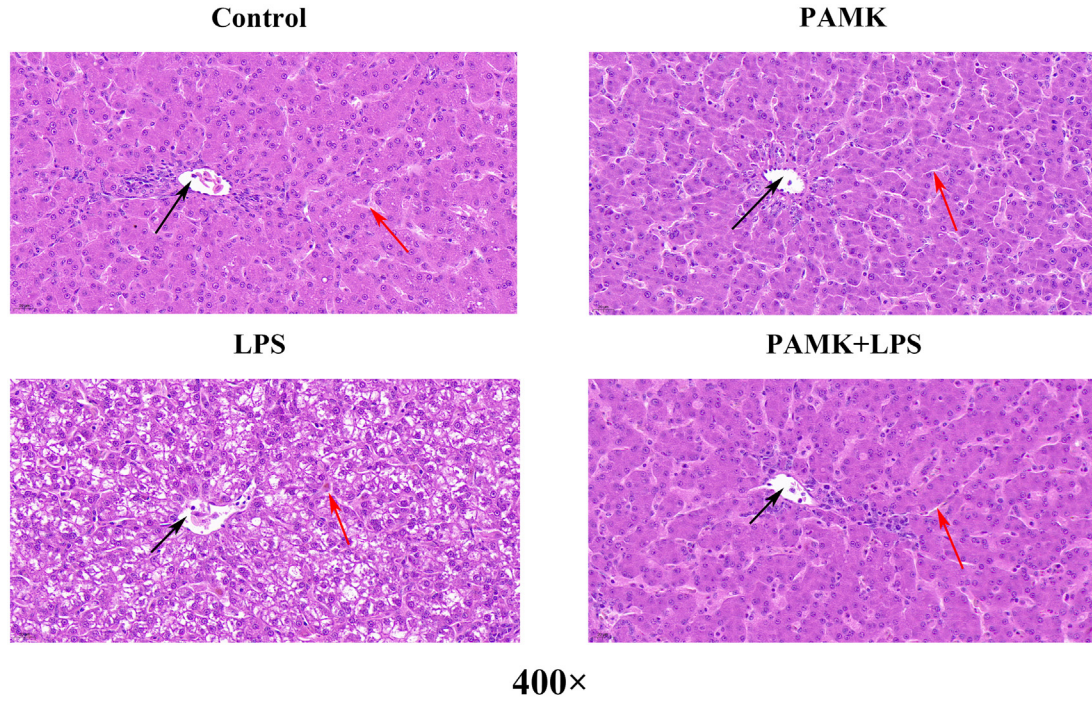
Control

PAMK

LPS

PAMK+LPS

400×

Figure 1. HE staining results of gosling livers (400 ×). The black arrow points to the central vein, and the red arrow points to the hepatic sinusoids.

Effect of PAMK on Biochemical Indices in the Livers of Goslings Induced by LPS

The levels of ALT and AST in the liver tissue of goslings were measured in all groups (Figure 2). The treatment group, with the addition of PAMK alone, had levels similar to those of the control group. The levels of ALT and AST in the livers of LPS-induced goslings were significantly higher than the control levels ($P <$ 0.05), while the addition of PAMK downregulated their levels to normal levels.

Transcriptome Data

To explore the pathways involved in the role of PAMK in alleviating LPS-induced liver injury in

goslings, liver tissues from goslings in the LPS and PAMK + LPS groups were selected, and the transcriptome was examined using the RNA-Seq method. As shown in Table 1, each sample generated 45.8 to 52.0 million raw read data, and after quality control filtering, each sample had 44.0 to 49.9 million valid read data, and the valid ratio (reads) of each sample was over 95.81. The base mass values of all samples ranged from 97.30% to 97.44%, and the percentage of GC content was 48.50%. The sample data were tested by several indicators and showed satisfactory results.

We describe the expression of the detected mRNAs in the liver of goslings. As shown in Figure 3(A), most of the mRNAs were between 1,000 and 3,500 bp in length, and the number of mRNAs greater than 6,000 bp in length was the largest. Meanwhile, the number of exons
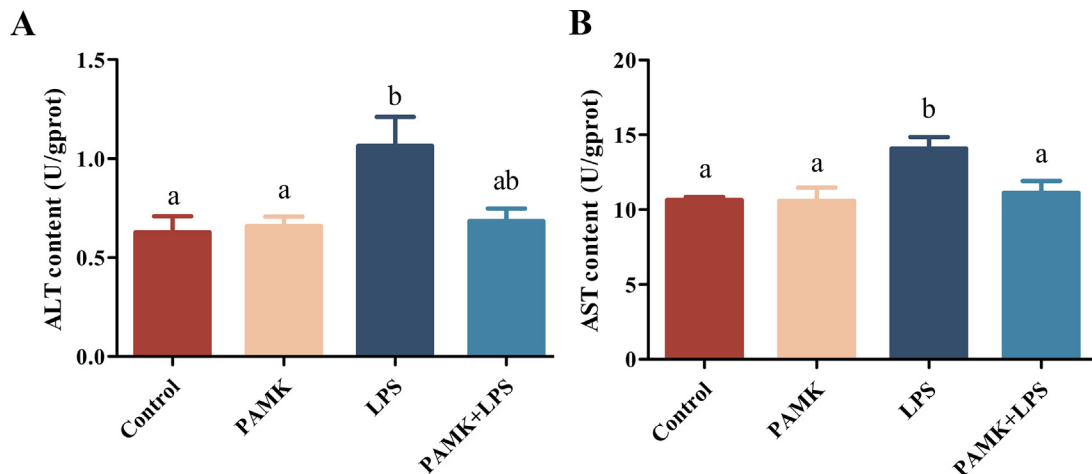
A

B

Figure 2. Effect of PAMK on LPS-induced ALT and AST in the livers of goslings. Data are expressed as the mean ± standard error (SEM). The data columns labeled with different lowercase letters indicate significant differences ($P < 0.05$), as in the following figure.

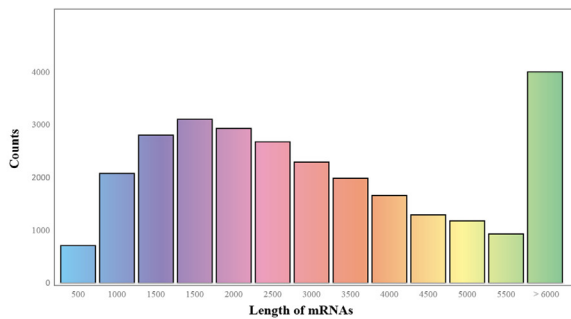**Table 1.** Quality analysis of transcriptome sequencing and mapping.

Sample	Raw data (read)	Valid data (read)	Valid ratio(reads)	Q30%	GC content%
LPS1	45825564	43990084	95.99	97.33	48.50
LPS2	49605102	47688432	96.14	97.41	48.50
LPS3	51768960	49660302	95.93	97.39	48.50
PAMK + LPS1	50432826	48344376	95.86	97.38	48.50
PAMK + LPS2	49565822	47562930	95.96	97.30	48.50
PAMK + LPS3	52053250	49871216	95.81	97.44	48.50

showed the same pattern, with the number of genes gradually decreasing as the number of exons increased, with the highest proportion of mRNAs with exon number 3 exceeding 10% (Figure 3B). We also performed a statistical analysis of the regional distribution of mRNAs for each sample, with similar percentages of different regions (Figure 3C).

Identification of Differentially Expressed Genes

Experiments were performed to analyze the sequencing data of gosling livers from the LPS and PAMK + LPS groups according to the $P < 0.05$ and |log2(FC)>1| criteria. In the scatter plot, blue dots indicate downregulated genes, red dots indicate upregulated genes, gray dots indicate nondifferentially expressed genes, and the size of the dots indicates the significance of genes. The larger the dots are, the stronger the significance. A total of 406 DEGs (242 upregulated and 164 downregulated) were identified (Figure 4).

Functional Analyses of DEGs

To further determine the mechanism of the protective effect of PAMK on LPS-induced liver injury in goslings,
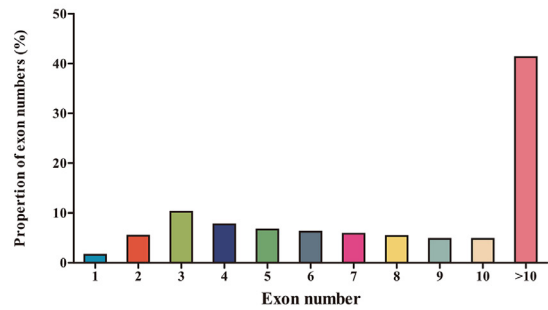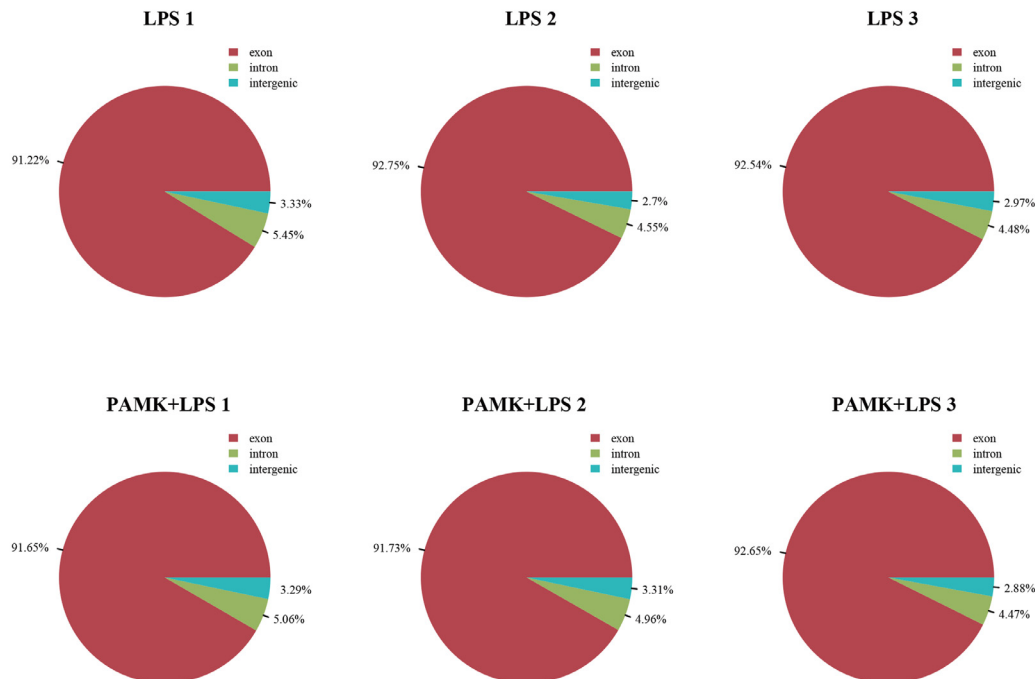

Figure 3. Expression of mRNA in the livers of goslings. (A) Length distribution of mRNAs. (B) Exon number distribution of mRNAs. (C) Description results of the regional distribution of mRNAs.
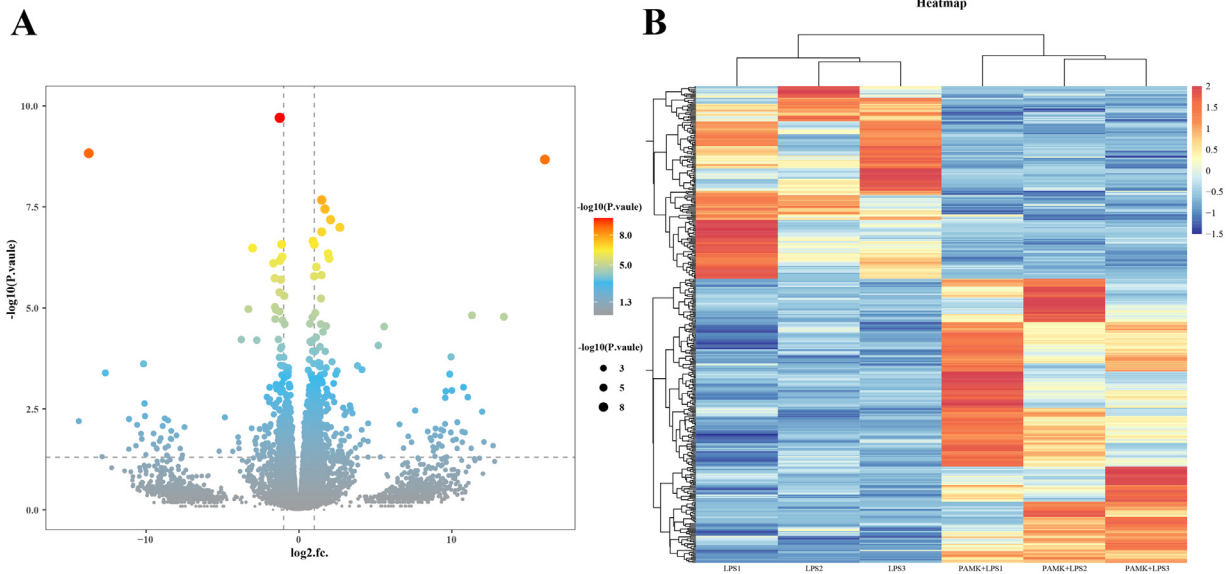
A

B

Figure 4. DEGs in the livers of the LPS and PAMK + LPS groups of goslings. (A)Volcano map of LPS vs. PAMK + LPS DEGs. (B) Heatmap of LPS vs. PAMK + LPS DEGs.

a functional enrichment analysis of DEGs was performed. As shown in Figure 5(A), the 50 GO terms were enriched in the LPS group compared with the PAMK +LPS group. These included 25 GO terms in the biological process (BP) category, 15 GO terms in the cellular component (CC) category, and 10 GO terms in the molecular function (MF) category. Among the 25 GO items significantly enriched by BP, the most enriched items were those related to immune processes such as lymphocyte chemotaxis, monocyte chemotaxis, cellular response to interleukin-1, positive regulation of B-cell activation, calcium-mediated signaling using intracellular calcium source, inflammatory response, and chemokine-mediated signaling pathway. Among the 15 GO

items significantly enriched by CC, DEGs were more involved in spindle midzone, condensed nuclear chromosome outer kinetochore, condensed chromosome, meiotic spindle, chromosome, centromeric region and cell cycle component related items. Among the 10 GO items significantly enriched in MF, DEGs were more enriched in chemokine activity, CCR chemokine receptor binding, and G protein-coupled peptide receptor activity related to chemokines ($P < 0.05$).

The results of the KEGG enrichment pathway analysis showed that DEGs were more enriched in the p53 signaling pathway, FOXO signaling pathway, and PPAR signaling pathway, which are pathways related to immune signaling (Figure 5B). In addition, pathways
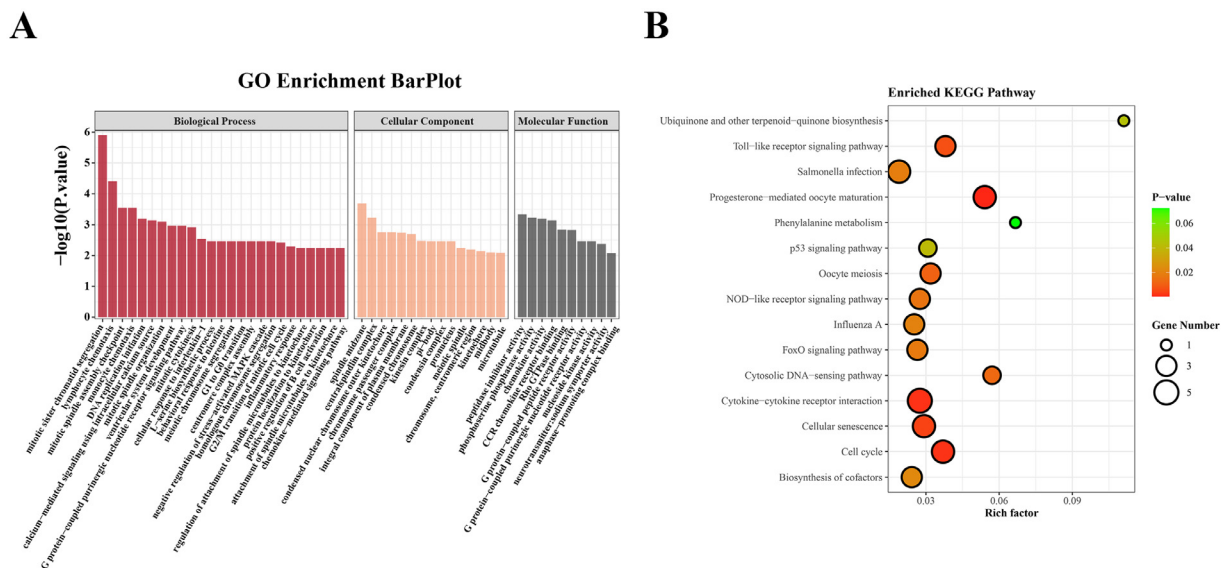
A

B

Figure 5. GO and KEGG pathway enrichment analyses of DEGs in gosling liver. (A) GO enrichment histogram of LPS vs. PAMK + LPS DEGs. (B) KEGG enrichment bubble plot of LPS vs. PAMK + LPS DEGs.
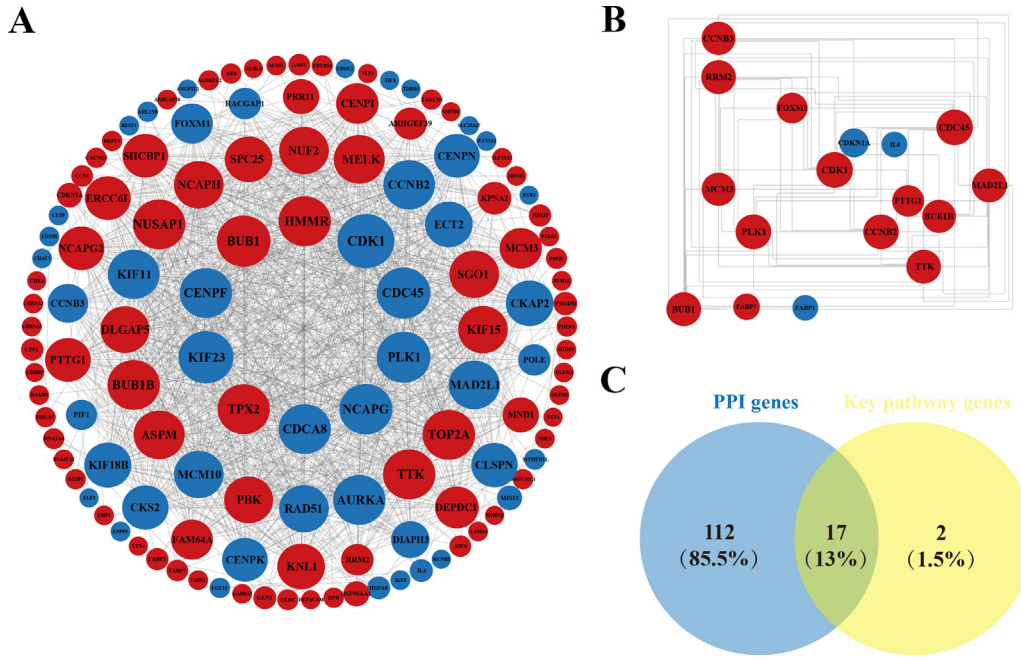
A

B

C

Figure 6. Interaction map of the differentially expressed protein–protein network. (A) PPI map of all DEGs. (B) PPI map of DEGs in 5 related signaling pathways. (C) Cross plot of all DEG in PPIs and DEGs in 5 related signaling pathways. The size of the circle shows the strength of the data support, with red representing upregulated genes and blue representing downregulated genes.

related to the cell cycle and cellular senescence were also included ($P < 0.05$).

PPI Network and Module Analysis

The STRING 10 database was used to construct PPI networks for all DEGs and to further analyze their possible modes of interaction. The results showed that 129 DEGs were correlated (Figure 6A). Among the 129 related DEGs, 17 DEGs were enriched in five related pathways: the p53 signaling pathway, FOXO signaling pathway, PPAR signaling pathway, cell cycle, and cellular sense (Figure 6B, C). Among them, CDK1, CDKN1A, RRM2, and CCNB2 are enriched in the p53 signaling pathway. The IL6, CCNB2, CDKN1A, CCNB3, and PLK1 genes are enriched in the FOXO signaling pathway. PPI network analysis confirmed that CDK1, CDKN1A, RRM2, CCNB2, IL6, CCNB3, and PLK1 have a strong biological interaction relationship.

Validation of RNA-Seq Results Using qRT–PCR

To determine the reliability of the RNA-Seq data, a fluorescence quantitative method was used to detect the expression levels of 7 DEGs enriched in the p53 signaling pathway and FOXO signaling pathway. As shown in Figure 7, in RNA-Seq and qRT–PCR, the changes in the expression of these DEGs showed the same upward or downward trend. Therefore, the RNA-Seq data are reliable, which also indicates that the p53 signaling pathway and FOXO signaling pathway may play important roles in PAMK-mediated relief of LPS-induced liver injury.

DISCUSSION

The liver is an important intrinsic immune organ in the body. The histomorphological structure of the liver reflects the degree of health of the liver. Therefore, the histomorphological integrity of the liver, the degree of
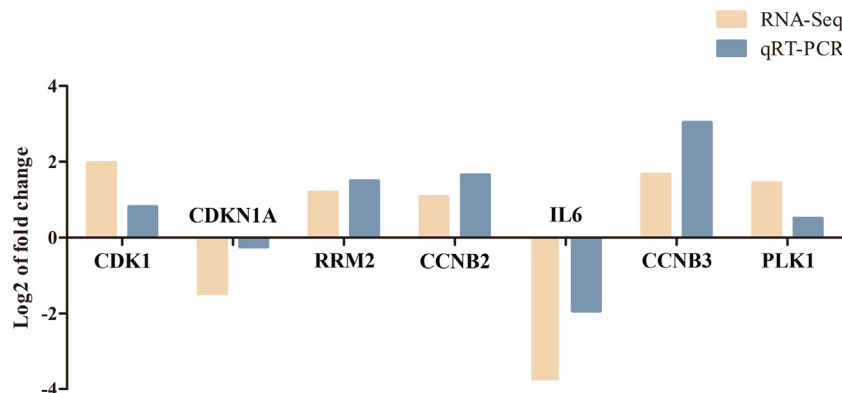

Figure 7. The results of qRT–PCR and RNA-seq for 7 DEGs from two comparison groups.

congestion or inflammatory infiltration, and thus the degree of liver health is assessed (Hermenean et al., 2012). In this experiment, LPS-induced liver damage in goslings with unclear hepatic cord structure and loss of hepatocyte cytoplasmic contents, and the LPS-induced liver damage was alleviated by PAMK after feeding PAMK. ALT and AST are markers of liver dysfunction and can also be used to evaluate hepatocyte inflammatory injury (Yang et al., 2017). LPS-induced liver damage and upregulated ALT and AST levels. Notably, PAMK was effective in alleviating LPS-induced damage to the liver tissue structure of goslings and maintaining normal levels of ALT and AST in liver tissue. This showed that PAMK helped to alleviate LPS-induced liver damage in goslings.

To further explore the mechanism by which PAMK alleviates LPS-induced liver injury in goslings, we screened DEGs in the liver tissues of goslings in the LPS and PAMK + LPS groups using RNA-Seq technology. The sequencing results showed that a total of 406 DEGs were detected in the liver tissues of goslings in the PAMK+LPS group compared to the LPS group. There were 242 upregulated genes and 164 downregulated genes. Further biofunctional interpretation of DEGs was performed using GO functional enrichment. The results showed that most of the DEGs were related to the immune response. The chemokine-mediated signaling pathway, chemokine activity, CCR chemokine receptor binding, and G protein-coupled peptide receptor activity suggest that the mitogenic effect of PAMK is associated with chemokine action. Chemokines are associated with immune responses. Chemokines are generally considered to be a group of cytokines that can be transcriptionally expressed under the influence of damage-associated molecular patterns or pathogen-associated molecular patterns to act as migratory or chemotactic agents for neutrophils or monocytes (Rollins, 1997; Bandow et al., 2012; Finney et al., 2012). When chemokines bind to their receptors, they can cause targeted migration or chemotaxis of leukocytes and regulate inflammation (Dinarello, 2007; Bhattacharya et al., 2020). In the present study, both lymphocytes and monocytes were involved in chemotaxis, and the binding of chemokines to their receptors and the activation of chemokine-mediated pathways showed the important role played by chemokines in PAMK remission. In addition, the cellular response to interleukin-1 and positive regulation of B-cell activation showed that immune cells are also involved in the mitigating effects of PAMK.

The results of KEGG enrichment pathways showed the top 15 enrichment pathways, including the p53 signaling pathway, FOXO signaling pathway, PPAR signaling pathway, cell cycle, and cellular senescence. In the p53 signaling pathway, p53 signaling is activated in response to stress or injury and can be involved in a variety of biological processes, such as the cell cycle, cellular senescence, and cellular metabolism, by regulating the expression of downstream target genes (Levine et al., 2009; Wang et al., 2013; Kim et al., 2017). It has been demonstrated in several publications that inflammation can be mitigated through the p53 signaling pathway (Chen et al., 2020; You et al., 2020). The FOXO family in the FOXO signaling pathway mediates a wide range of physiological functions, including oxidative stress, cell metabolism, and autophagic apoptosis (Kops et al., 2002; Modur et al., 2002; Puigserver et al., 2003). The FOXO family-mediated signaling pathway has been documented to mitigate oxidative stress and apoptosis, thereby regulating the liver (Tao et al., 2013; Mahmoud et al., 2019).

The DEGs in these five signaling pathways intersected with 129 interrelated genes in the PPI network to obtain 17 DEGs. Among them, CDK1, CDKN1A, RRM2, CCNB2, IL6, CCNB3, and PLK1 were enriched in the p53 signaling pathway and FOXO signaling pathway. To further determine the mechanism of action of PAMK in alleviating LPS-induced liver injury in goslings, qRT–PCR validation of these DEGs were performed to confirm the plausibility of the RNA-Seq data. CDK1 proteins are cyclin-dependent kinases that are involved in regulating the G2/M regulatory network of the cell cycle and are important in driving mitosis (Evan et al., 2001; Diril et al., 2012). CDK1 gene expression can be involved in the pathogenesis of rheumatoid arthritis and the process of cardiac inflammation and fibrosis (Garcia-Martin et al., 2021; Fattah et al., 2022). CDKN1A, also known as p21, can be transcriptionally activated by p53 (Engeland, 2022). In the presence of telomere damage, CDKN1A is able to restore cellular homeostasis by inhibiting the activity of CDK1, causing cell cycle arrest and DNA repair (Ou et al., 2018). However, overexpression of the CDKN1A gene can block the cell cycle, resulting in a series of cellular senescence phenomena (Johnson et al., 2018). In mice, the CDKN1A gene has been shown to be an inflammatory response gene in the central nervous system (Ring et al., 2003). RRM2 is a ribonucleotide reductase involved in the regulation of DNA synthesis and repair (Ma et al., 2020). RRM2 also shows significant differences in macrophage polarization (Li et al., 2022). CCNB is a member of the cell cycle protein family and plays an important role in cell division (Hong et al., 2021). A total of 3 CCNBs were identified in the avian population, namely, CCNB1, CCNB2, and CCNB3 (Gao et al., 2020; Yang et al., 2020). CCNB can form a complex with CDK1 and plays a key role in the cell cycle G2/M regulatory network (Malumbres et al., 2005). IL6 is an inflammatory cytokine that binds to its receptor and triggers the activation of the JAK/STAT signaling pathway (Zhang et al., 2019). Significant downregulation of IL6 gene expression mitigated murine liver injury, along with decreased acetylation of FOXO (Binmowyna et al., 2021). It has also been demonstrated that phosphorylation of FOXO can trigger inflammatory signaling pathways and that its levels correlate with the expression of the cellular inflammatory factor IL6 (Li et al., 2017). PLK1 is a serine/threonine protein kinase that plays an important regulatory role in the cell cycle (Cao et al., 2021). PLK1 can mediate a variety of
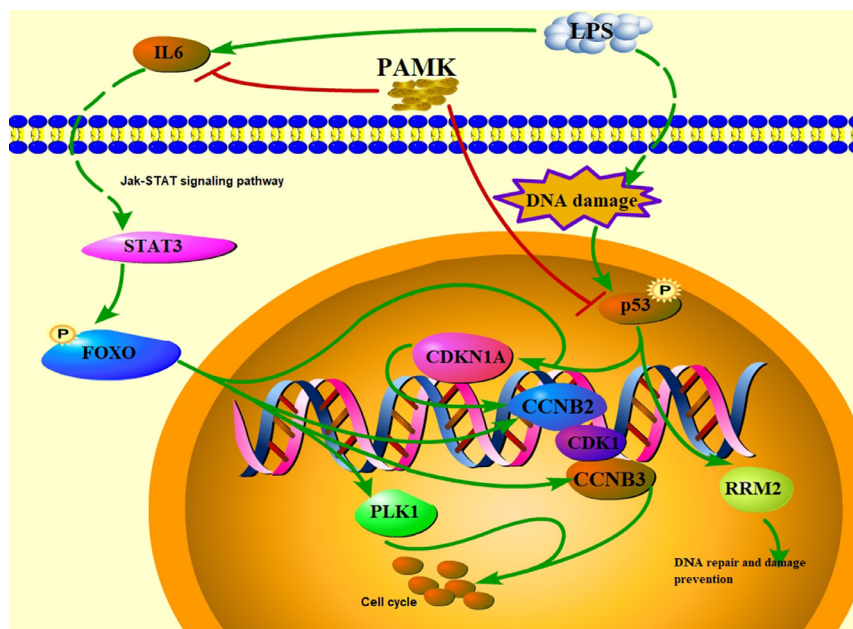
Figure 8. Diagram of the p53 and FOXO signaling pathways.

functions in vivo, such as DNA replication and various stress response processes (Vertii et al., 2016). In the DEGs validated in this study, CDK1, CCNB2, RRM2, and CDKN1A were enriched in the p53 signaling pathway, which is involved with the cell cycle and DNA damage repair. In addition, in the FOXO signaling pathway, IL6 can act as an inflammatory cytokine, activating the pathway and regulating downstream CCNB2, CCNB3, PLK1, and CDKN1A, which in turn exert immune effects. According to the importance of these two pathways in injury, PAMK may alleviate LPS-induced liver injury through the p53 signaling pathway and the FOXO signaling pathway.

In conclusion, PAMK may regulate the levels of ALT and AST in liver tissue through the p53 signaling pathway and FOXO signaling pathway to maintain the morphological and structural integrity of the liver, thereby attenuating LPS-induced liver injury in goslings (Figure 8).

ACKNOWLEDGMENTS

DISCLOSURES

The authors declare no conflicts of interest.

REFERENCES

Bandow, K., J. Kusuyama, M. Shamoto, K. Kakimoto, T. Ohnishi, and T. Matsuguchi. 2012. Lps-induced chemokine expression in both myd88-dependent and -independent manners is regulated by cot/tpl2-erk axis in macrophages. Febs. Lett. 586:1540–1546.

Beutler, B. 2004. Inferences, questions and possibilities in toll-like receptor signalling. Nature 430:257–263.

Bhattacharya, S., and A. Kawamura. 2020. Using evasins to target the chemokine network in inflammation. Adv. Protein Chem. Struct. Biol. 119:1–38.

Bilodeau-Bourgeois, L., B. G. Bosworth, and B. C. Peterson. 2008. Differences in mortality, growth, lysozyme, and toll-like receptor gene expression among genetic groups of catfish exposed to virulent edwardsiella ictaluri. Fish Shellfish Immunol. 24:82–89.

BinMowyna, M. N., and N. A. AlFaris. 2021. Kaempferol suppresses acetaminophen-induced liver damage by upregulation/activation of sirt1. Pharm. Biol. 59:146–156.

Bowen, O. T., R. L. Dienglewicz, R. F. Wideman, and G. F. Erf. 2009. Altered monocyte and macrophage numbers in blood and organs of chickens injected i.v. With lipopolysaccharide. Vet. Immunol. Immunopathol. 131:200–210.

Cao, Y. Y., Z. Wang, T. Yu, Y. Zhang, Z. H. Wang, Z. M. Lu, W. H. Lu, and J. B. Yu. 2021. Sepsis induces muscle atrophy by inhibiting proliferation and promoting apoptosis via plk1-akt signalling. J. Cell Mol. Med. 25:9724–9739.

Chastre, A., M. Belanger, B. N. Nguyen, and R. F. Butterworth. 2014. Lipopolysaccharide precipitates hepatic encephalopathy and increases blood-brain barrier permeability in mice with acute liver failure. Liver Int. 34:353–361.

Chen, M., Z. Chen, D. Huang, C. Sun, J. Xie, T. Chen, X. Zhao, Y. Huang, D. Li, B. Wu, and D. Wu. 2020. Myricetin inhibits tnf-alpha-induced inflammation in a549 cells via the sirt1/nf-kappab pathway. Pulm. Pharmacol. Ther. 65:102000.

Dinarello C.A., Historical insights into cytokines, *Eur. J. Immunol.*, 37, 2007, S34−S45.

Ding, Y., P. Liu, Z. L. Chen, S. J. Zhang, Y. Q. Wang, X. Cai, L. Luo, X. Zhou, and L. Zhao. 2018. Emodin attenuates lipopolysaccharide-induced acute liver injury via inhibiting the tlr4 signaling pathway in vitro and in vivo. Front Pharmacol. 9:962.

Diril, M. K., C. K. Ratnacaram, V. C. Padmakumar, T. Du, M. Wasser, V. Coppola, L. Tessarollo, and P. Kaldis. 2012. Cyclin-dependent kinase 1 (cdk1) is essential for cell division and suppression of dna re-replication but not for liver regeneration. Proc. Natl. Acad. Sci. U. S. A. 109:3826–3831.

Engeland, K. 2022. Cell cycle regulation: p53-p21-rb signaling. Cell Death Differ. 29:946–960.

Evan, G. I., and K. H. Vousden. 2001. Proliferation, cell cycle and apoptosis in cancer. Nature 411:342–348.

Fattah, S. A., F. M. Abdel, N. M. Mesbah, S. M. Saleh, D. M. Abo-Elmatty, and E. T. Mehanna. 2022. The expression of

zinc finger 804a (znf804a) and cyclin-dependent kinase 1 (cdk1) genes is related to the pathogenesis of rheumatoid arthritis. Arch. Physiol. Biochem. 128(3):688–693.

Finney, S. J., S. K. Leaver, T. W. Evans, and A. Burke-Gaffney. 2012. Differences in lipopolysaccharide- and lipoteichoic acid-induced cytokine/chemokine expression. Intensive Care Med. 38:324–332.

Gao, J., Z. Gao, F. Dang, X. Li, H. Liu, X. Liu, M. Gao, and J. Ruan. 2020. Calcium promotes differentiation in ameloblast-like ls8 cells by downregulation of phosphatidylinositol 3 kinase /protein kinase b pathway. Arch. Oral. Biol. 109:104579.

Garcia-Martin, A., C. Navarrete, M. Garrido-Rodriguez, M. E. Prados, D. Caprioglio, G. Appendino, and E. Munoz. 2021. Ehp-101 alleviates angiotensin ii-induced fibrosis and inflammation in mice. Biomed. Pharmacother. 142:112007.

Guo, S., W. Li, F. Chen, S. Yang, Y. Huang, Y. Tian, D. Xu, and N. Cao. 2021. Polysaccharide of atractylodes macrocephala koidz regulates lps-mediated mouse hepatitis through the tlr4-myd88-nfkappab signaling pathway. Int. Immunopharmacol 98:107692.

Hermenean, A., C. Popescu, A. Ardelean, M. Stan, N. Hadaruga, C. V. Mihali, M. Costache, and A. Dinischiotu. 2012. Hepatoprotective effects of berberis vulgaris l. Extract/beta cyclodextrin on carbon tetrachloride-induced acute toxicity in mice. Int. J. Mol. Sci. 13:9014–9034.

Hong, Z., Q. Wang, C. Hong, M. Liu, P. Qiu, R. Lin, X. Lin, F. Chen, Q. Li, L. Liu, C. Wang, and D. Chen. 2021. Identification of seven cell cycle-related genes with unfavorable prognosis and construction of their tf-mirna-mrna regulatory network in breast cancer. J. Cancer 12:740–753.

Johnson, A. C., and R. A. Zager. 2018. Plasma and urinary p21: potential biomarkers of aki and renal aging. Am. J. Physiol. Renal. Physiol. 315:F1329–F1335.

Kim, G. J., D. H. Song, H. S. Yoo, K. H. Chung, K. J. Lee, and J. H. An. 2017. Hederagenin supplementation alleviates the pro-inflammatory and apoptotic response to alcohol in rats. Nutrients 9:41.

Kops, G. J., T. B. Dansen, P. E. Polderman, I. Saarloos, K. W. Wirtz, P. J. Coffer, T. T. Huang, J. L. Bos, R. H. Medema, and B. M. Burgering. 2002. Forkhead transcription factor foxo3a protects quiescent cells from oxidative stress. Nature 419:316–321.

Levine, A. J., and M. Oren. 2009. The first 30 years of p53: growing ever more complex. Nat. Rev. Cancer. 9:749–758.

Li, B. X., W. Y. Li, Y. B. Tian, S. X. Guo, Y. M. Huang, D. N. Xu, and N. Cao. 2019. Polysaccharide of atractylodes macrocephala koidz enhances cytokine secretion by stimulating the tlr4-myd88-nf-kappab signaling pathway in the mouse spleen. J. Med. Food 22:937–943.

Li, N., X. Wang, X. Wang, H. Yu, L. Lin, C. Sun, P. Liu, Y. Chu, and J. Hou. 2017. Upregulation of foxo 1 signaling mediates the proinflammatory cytokine upregulation in the macrophage from polycystic ovary syndrome patients. Clin. Lab. 63:301–311.

Li, W., X. Xiang, B. Li, Y. Wang, L. Qian, Y. Tian, Y. Huang, D. Xu, and N. Cao. 2021. Pamk relieves lps-induced enteritis and improves intestinal flora disorder in goslings. Evid. Based Complement Alternat. Med. 2021:9721353.

Li, W., X. Zhou, S. Xu, N. Cao, B. Li, W. Chen, B. Yang, M. Yuan, and D. Xu. 2022. Lipopolysaccharide-induced splenic ferroptosis in goslings was alleviated by polysaccharide of atractylodes macrocephala koidz associated with proinflammatory factors. Poult. Sci. 101:101725.

Li, X. C., S. J. Luo, W. Fan, T. L. Zhou, D. Q. Tan, R. X. Tan, Q. Z. Xian, J. Li, C. M. Huang, and M. S. Wang. 2022. Macrophage polarization regulates intervertebral disc degeneration by modulating cell proliferation, inflammation mediator secretion, and extracellular matrix metabolism. Front. Immunol. 13:922173.

Lindros, K. O., and H. A. Jarvelainen. 2005. Chronic systemic endotoxin exposure: an animal model in experimental hepatic encephalopathy. Metab. Brain Dis. 20:393–398.

Liu, X., P. Y Guan, C. T. Yu, H. Yang, A. S. Shan, and X. J. Feng. 2022. Curcumin alleviated lipopolysaccharide-induced lung injury via regulating the nrf2-are and nf-kappab signaling pathways in ducks. J. Sci. Food. Agric. 102:6603–6611.

Ma, C., H. Luo, J. Cao, C. Gao, X. Fa, and G. Wang. 2020. Independent prognostic implications of rrm2 in lung adenocarcinoma. J. Cancer. 11:7009–7022.

Mahmoud, A. R., F. Ali, T. H. Abd-Elhamid, and EHM. Hassanein. 2019. Coenzyme q10 protects hepatocytes from

ischemia reperfusion-induced apoptosis and oxidative stress via regulation of bax/bcl-2/puma and nrf-2/foxo-3/sirt-1 signaling pathways. Tissue Cell. 60:1–13.

Malumbres, M., and M. Barbacid. 2005. Mammalian cyclin-dependent kinases. Trends Biochem. Sci. 30:630–641.

Miao, Y. F., X. N. Gao, D. N. Xu, M. C. Li, Z. S. Gao, Z. H. Tang, N. H. Mhlambi, W. J. Wang, W. T. Fan, X. Z. Shi, G. L. Liu, and S. Q. Song. 2021. Protective effect of the new prepared atractylodes macrocephala koidz polysaccharide on fatty liver hemorrhagic syndrome in laying hens. Poult. Sci. 100:938–948.

Modur, V., R. Nagarajan, B. M. Evers, and J. Milbrandt. 2002. Foxo proteins regulate tumor necrosis factor-related apoptosis inducing ligand expression. Implications for pten mutation in prostate cancer. J. Biol. Chem. 277:47928–47937.

Ou, H. L., and B. Schumacher. 2018. Dna damage responses and p53 in the aging process. Blood 131:488–495.

Puigserver, P., J. Rhee, J. Donovan, C. J. Walkey, J. C. Yoon, F. Oriente, Y. Kitamura, J. Altomonte, H. Dong, D. Accili, and B. M. Spiegelman. 2003. Insulin-regulated hepatic gluconeogenesis through foxo1-pgc-1alpha interaction. Nature 423:550–555.

Qin, S., W. Bai, T. J. Applegate, K. Zhang, G. Tian, X. Ding, S. Bai, J. Wang, L. Lv, H. Peng, Y. Xuan, and Q. Zeng. 2022. Dietary resistant starch ameliorating lipopolysaccharide-induced inflammation in meat ducks associated with the alteration in gut microbiome and glucagon-like peptide 1 signaling. J. Anim. Sci. Biotechnol. 13:91.

Quiroz, S. C., L. Bucio, V. Souza, E. Hernandez, E. Gonzalez, L. Gomez-Quiroz, D. Kershenobich, F. Vargas-Vorackova, and M. C. Gutierrez-Ruiz. 2001. Effect of endotoxin pretreatment on hepatic stellate cell response to ethanol and acetaldehyde. J. Gastroenterol. Hepatol. 16:1267–1273.

Ring, R. H., Z. Valo, C. Gao, M. E. Barish, and J. Singer-Sam. 2003. The cdkn1a gene (p21waf1/cip1) is an inflammatory response gene in the mouse central nervous system. Neurosci. Lett. 350:73–76.

Rollins, B. J. 1997. Chemokines. Blood. 90:909–928.

Tao, G. Z., N. Lehwald, K. Y. Jang, J. Baek, B. Xu, M. B. Omary, and K. G. Sylvester. 2013. Wnt/beta-catenin signaling protects mouse liver against oxidative stress-induced apoptosis through the inhibition of forkhead transcription factor foxo3. J. Biol. Chem. 288:17214–17224.

Vertii, A., M. Ivshina, W. Zimmerman, H. Hehnly, S. Kant, and S. Doxsey. 2016. The centrosome undergoes plk1-independent interphase maturation during inflammation and mediates cytokine release. Dev. Cell. 37:377–386.

Wang, X., X. Zhao, X. Gao, Y. Mei, and M. Wu. 2013. A new role of p53 in regulating lipid metabolism. J. Mol. Cell Biol. 5:147–150.

Xi, Y., J. Yan, M. Li, S. Ying, and Z. Shi. 2019. Gut microbiota dysbiosis increases the risk of visceral gout in goslings through translocation of gut-derived lipopolysaccharide. Poult. Sci. 98:5361–5373.

Xu, D., and Y. Tian. 2015. Selenium and polysaccharides of atractylodes macrocephala koidz play different roles in improving the immune response induced by heat stress in chickens. Biol. Trace Elem. Res. 168:235–241.

Yang, H., Y. Wang, M. Liu, X. Liu, Y. Jiao, S. Jin, A. Shan, and X. Feng. 2021. Effects of dietary resveratrol supplementation on growth performance and anti-inflammatory ability in ducks (anas platyrhynchos) through the nrf2/ho-1 and tlr4/nf-kappab signaling pathways. Animals (Basel) 11.

Yang, Q., G. Ji, R. Pan, Y. Zhao, and P. Yan. 2017. Protective effect of hydrogen-rich water on liver function of colorectal cancer patients treated with mfolfox6 chemotherapy. Mol. Clin. Oncol. 7:891–896.

Yang, S. Y., H. Ren, C. F. Li, C. F. Li, and H. Tang. 2020. Screening core genes and cyclin b2 as a potential diagnosis, treatment and prognostic biomarker of hepatocellular carcinoma based on bioinformatics analysis. Zhonghua Gan Zang Bing Za Zhi 28:773–783.

You, M., Z. Miao, O. Sienkiewicz, X. Jiang, X. Zhao, and F. Hu. 2020. 10-hydroxydecanoic acid inhibits lps-induced inflammation by targeting p53 in microglial cells. Int. Immunopharmacol. 84:106501.

Zhang, L. J., S. Z. Ni, X. L. Zhou, and Y. Zhao. 2019. Hemorrhagic shock sensitized the diaphragm to ventilator-induced dysfunction through the activation of il-6/jak/stat signaling-mediated autophagy in rats. Mediators Inflamm. 2019:3738409.